ELSEVIER

Materials Science and Engineering B99 (2003) 541–548

MATERIALS SCIENCE & ENGINEERING B

www.elsevier.com/locate/mseb

Simulation of grain growth for ABO_3 type ceramics

Z.X. Xiong [a,*], G.L. Ji [b], X. Fang [b]

[a] *Department of Materials Science and Engineering, Xiamen University, Xiamen 361005, People's Republic of China*
[b] *Department of Automation, Xiamen University, Xiamen 361005, People's Republic of China*

Abstract

The evolutions of grain growth in ceramics with ABO_3 type structure were simulated at atomistic level by the Monte Carlo method with Visual C++ language. Several parameters, such as initial seed number, seed activation coefficient, sintering temperature and time, were incorporated. Realistic images in series were monitored and quantitative data were obtained, including the fractal dimensions of grain boundaries during the kinetic evolution of grain growth. The resulted kinetic exponents of grain growth were variable during the process of simulation, being smaller (~ 1.8) at early period and larger (~ 5.5) at later stage. It was in good agreement with the experimental result of practical $(Ba_{0.9}Sr_{0.1})TiO_3$ ceramics.

Keywords: Simulation; Grain growth; ABO_3 ceramics; Monte Carlo method; Kinetic exponent

1. Introduction

It is now established that there is a strong correlation between the physical properties of ceramics and their microstructures, which result mainly from the grain growth process [1–3]. Therefore, the study of grain growth during the microstructural evolution is of fundamental importance [4–6]. Grain growth is a process by which the average grain size or area increases with time in a material, usually at high temperature. One of the most important driving forces results from the decrease in the total free energy of grain boundaries, which accompanies reduction in the total boundary area [7]. This force drives the boundary to migrate towards its curvature center. Consequently, larger grains grow at the expense of smaller grains that diminish in size and even disappear. Other driving forces may originate from the difference in the volume free energy between the grains on either side of a grain boundary, due to difference in chemical composition, defect density, or grain orientation.

Recently a variety of computer simulation techniques have been developed to describe grain growth in polycrystalline materials. The most widespread approach to model grain growth is based on a Monte Carlo technique, usually formulated as a Potts model [6,8]. Area in two-dimension or volume in three-dimension is divided into separate pixels, each of which is assigned a particular grain identity characterized as a state. The migration of grain boundary is achieved, by changing the grain identity of pixels that adjoin the boundary. The pixel chosen at random is then allowed to change its state so as to minimize energy, with a probability defined by a Boltzmann distribution of probable states according to their energy levels. Having the same state as neighboring pixels gives a lower energy, while having a different state produce a higher energy. Grain boundaries move as the pixels at the boundaries change states. The energetics of grain growth is addressed through modification of interaction energies. The advantage of the Potts model is that it is very easy to extend to 3D, in addition to easy to code. Limitations are however as follows: large simulations are required to obtain truly accurate results, arbitrary curvature–velocity relationships are not easy to define, and detailed configuration at atomistic level can not be obtained.

In this paper, the simulation of grain growth at atomistic level is achieved for the ceramics with ABO_3 type structure. One of the distinctive advantages in this study is that realistic images in series during grain growth process can be monitored at atomistic level.

* Corresponding author
E-mail address: zxxiong@xmu.edu.cn (Z.X. Xiong).

0921-5107/02/$ - see front matter © 2002 Published by Elsevier Science B.V.
PII: S0921-5107(02)00551-2

For example, the mismatching of ions within grain boundaries can be clearly distinguished, as well as the different configurations of ions in different grains with different orientations. Another advantage is that several kinds of data can be simultaneously obtained, such as ion numbers, grain boundary length and even the evolution of fractal dimensions of grain boundaries in different grains.

2. Theory

2.1. Representation of ABO_3 structure ceramic

Fig. 1 shows a unit cell of ABO_3 structure with three different ions, A^{2+}, B^{4+} and O^{2-}. Ceramics with such structure are typical materials with usually ferroelectric behavior [9–11]. They belong to generally perovskite structure, such as $BaTiO_3$, $SrTiO_3$ and $PbZrO_3$ [12,13]. There is a ferroelectric–paraelectric phase transition at the Curie temperature (Tc).

During the simulations the three different ions in ABO_3 type ceramics are represented by different radii and colors. Projections along three typical lattice plane [001], [011] and [111] are displayed in Fig. 2 with three different shapes, i.e., square, rectangle and hexagon. Consequently, it is quite convenient to see in details configurations of ions not only in the areas of grain center but also in the regions of grain boundaries.

Therefore, the possible coordinates of $P'(x', y')$ for a new ion around the present ion of type A, with coordinates of $P(x, y)$, in a grain with random orientation of angle a can be calculated in following way.

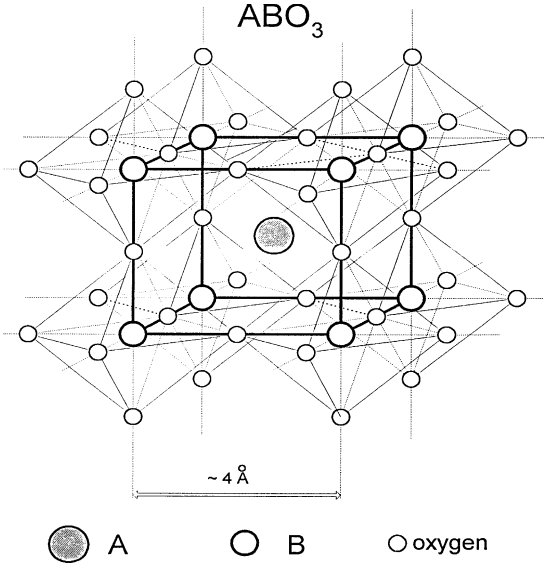

Fig. 1. Unit cell of ABO_3 structure ceramics.

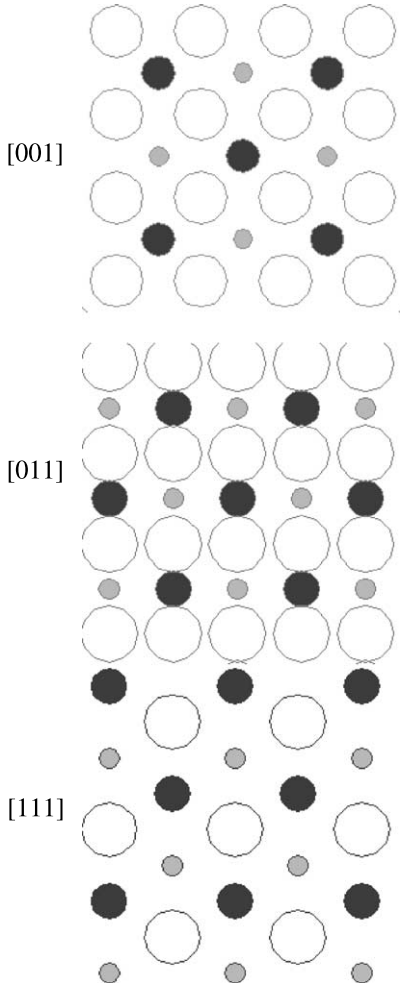

Fig. 2. Projections along lattice plane [001], [011] and [111] of ABO_3 structure ceramics.

$$\left.\begin{aligned} x' &= x + |PP'| * \cos\left(\alpha + \left(\prod/2\right) * \text{rand}\right) \\ y' &= y + |PP'| * \sin\left(\alpha + \left(\prod/2\right) * \text{rand}\right) \end{aligned}\right\}$$

here $|PP'| = a_0 * \sqrt{2}/2 * r$, a_0 is the constant of unit cell, r is the ionic radius, rand = 1 or 3 if P' belong to the ion of type B, and, rand = 0 or 2 if P' belong to the ion of type O for [001] lattice plane. Other cases can be deduced in similar way.

In three-dimension, an ion, $P(x, y, z)$, of type A in ABO_3 structure is neighbored with eight ions of type B and 12 ions of type O. The coordinates of possible new ions, $P'(x', y', z')$, can be then obtained,

$$\begin{cases} x' = x + P_P' \mathrm{d}x[\text{rand}] * r * a_0 \\ y' = y + P_P' \mathrm{d}y[\text{rand}] * r * a_0 \\ z' = z + P_P' \mathrm{d}z[\text{rand}] * r * a_0 \end{cases}$$

here a_0 is the constant of unit cell, r is the ionic radius, rand is a integer (0–19) representing different position

of new ions P' related with ion P, and, P_P' dx[rand], P_P' dy[rand] and P_P' dz[rand] are relative distances between ions P and P'.

As the orientations of different grains in ceramics are usually random, the direction of them can be expressed by three angles, i.e. Eulerian angles ψ, Φ and θ ($0 < \psi$, Φ, $\theta < 2\pi$). Consequently, the coordinates of possible new ions can be transformed as follows.

$$\begin{cases} x = x'(\cos\phi\cos\psi - \sin\phi\sin\psi\cos\theta) + y'(-\sin\phi\cos\psi - \cos\phi\sin\psi\cos\theta) + z'\sin\psi\sin\theta \\ y = x'(\cos\phi\sin\psi + \sin\phi\cos\psi\cos\theta) + y'(-\sin\phi\sin\psi + \cos\phi\cos\psi\cos\theta) - z'\cos\psi\sin\theta \\ z = x'\sin\phi\sin\theta + y'\cos\phi\sin\theta + z'\cos\theta \end{cases}$$

2.2. Interactive forces between ions

For any of ions in the ceramics, it is situated within electrostatic interaction of neighboring ions. For example, the interactive force of an ion with dark colors in Fig. 3 can be expressed with Coulomb interactive force as followings.

$$\mathrm{F} = -\left(k\frac{Q_1Q_2}{r^2} + k\frac{Q_1Q_3}{4r^2} + k\frac{Q_1Q_4}{9r^2} + k\frac{Q_1Q_5}{16r^2} + k \times \frac{Q_1Q_6}{25r^2}\cdots\right)$$

It can be seen that the contribution of the force decreases quickly with the increasing of distance, r, between ions. Therefore it is reasonable to neglect the interaction with ions far away. Resultant force along a certain direction of θ can then be obtained,

$$F_x = \sum_i F_i\cos\theta_i$$

$$F_y = \sum_i F_i\sin\theta_i$$

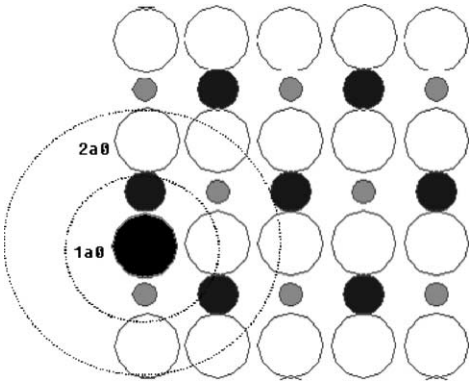

Fig. 3. Diagram for interactive force of ion in two-dimension.

Moreover, Fig. 4 shows that electrostatic interactions for the ions within grain boundary result from not only the ions in the same grain but also the ones in neighboring grains. The interactive force is thus expressed in this way.

$$F_x = F_{ix} + F_{ox} = -kQ_1\left(\sum_i \cos\theta_i \sum_n \frac{Q_n}{n^2r_i^2} + \cos\theta_l \sum_j \frac{Q_j}{l_j^2}\right)$$

$$F_y = F_{iy} + F_{oy} = -kQ_1\left(\sum_i \sin\theta_i \sum_n \frac{Q_n}{n^2r_i^2} + \sin\theta_l \sum_j \frac{Q_j}{l_j^2}\right)$$

Here, i is a line passing the considered ion (dark color), n is an ion on the line, l is a distance between the considered ion and an ion in a neighboring grain, θ_i is an angle between the line i and the coordinate axis, and θ_l is an angle between the line connecting the considered ion and an ion in a neighboring grain, and the coordinate axis.

In three-dimension, the interactive force of an ion (Fig. 5) is written as following.

$$F = kQ_1\sum_i\left(\frac{Q_i}{(Nr)^2 + R_i^2}\frac{Nr}{\sqrt{(Nr)^2 + R_i^2}}\right) = kQ_1\sum_i\left(\frac{Q_iNr}{[(Nr)^2 + R_i^2]^{\frac{3}{2}}}\right)$$

Here, i is the ion number, Q_i is the charge of the ion, R_i is a distance between ions, r is a minimum distance between ions.

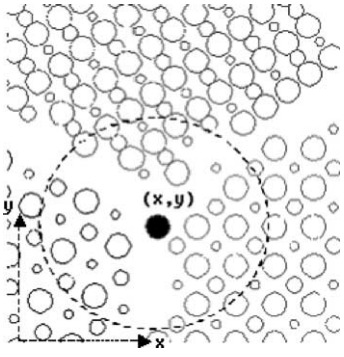

Fig. 4. Electrostatic interactions of ions in grain boundary.

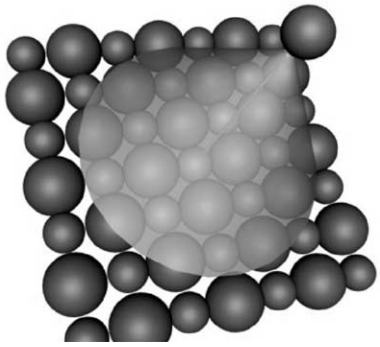

Fig. 5. Diagram for interactive force of ions in three-dimension.

2.3. Flow-chart of simulation of grain growth

As the true nature of the grain growth process may lie somewhere between growth driven by the grain boundary curvature and a random walk process [14]. In this paper, therefore, both of them have been incorporated into the programs of simulation, to achieve a realistic simulation of grain growth process. The former is achieved by a deterministic calculation to simulate the diffusion process. In this case mainly the direction of ions across a grain boundary, driven by the release of free energy as the ions move across the boundary from the convex surface to the concave surface. Alternatively, the driving force originates from a position with higher chemical potential to another with lower one. The latter is employed by the Monte Carlo methods with a certain probability, to model the random process that ions in the matrix transport onto the grain boundaries. In addition, ions jump from one grain to a neighboring grain due to thermal activation.

The flow-chart of the simulation for grain growth in ceramics is thus displayed as following.

There are actually two major steps for the simulations at atomistic level. The first step is to randomly produce the initial seed positions. The second step is to let the seeds grow according to the basic principles of grain growth process. For examples, the movement direction of ion is towards the center of the boundary curvature, and the probability of ionic jumping across a boundary is inversely proportional to the principal radii of the curvature, and is exponentially proportional to the temperature.

Table 1
Values of parameters used

Initial seed number (N_0)	5	10	15	20
Seed activation coefficient (α)	0	0.25	0.50	0.75
Sintering temperature (T)	1100	1200	1300	1400
Sintering time (t)	100	200	300	400
Ion radius (r)	0.05	0.10	0.15	0.20

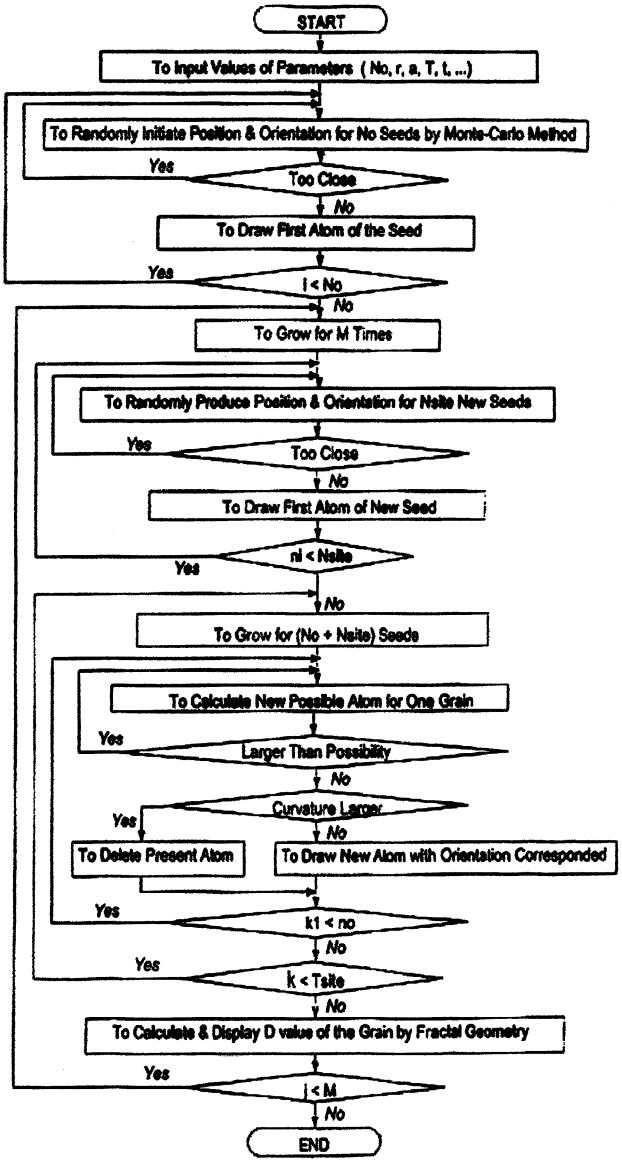

Several values of the different parameters have been used to simulate images for the optimization of microstructure at atomistic level. The parameters are described as follows. Initial seed number (N_0) is the number of seeds to be grown. Seed activation coefficient (α) is a parameter to represent the rate producing new seeds during the grain growth in which new seeds number $N = N_0 \exp(-\alpha T)$. Sintering temperature (T) corresponds to the temperature in practical ceramic sintering, which also contributes to the probability of ionic jumping across a boundary. Sintering time (t) indicates the soaking time in practical ceramic sintering and here is equal to the cycles of growth for all of the ions in whole system. Table 1 shows the values of parameters selected. The detailed results are discussed as follows.

2.4. Kinetic exponent of grain growth

Using a phenomenological approach, Burke and Turnbull deduced a parabolic relationship for grain growth kinetics [15], as following,

$$R_t^2 - R_0^2 = C_0 t$$

where R_t is the average grain size at time t, R_0 is the initial average grain size, and C_0 is a constant. After a longer growth time, there is usually $R_t \gg R_0$, therefore

$$R_t^2 \approx C_0 t$$

As experimental results [16–18] deviate in general from the above parabolic law, a more general expression is usually written as

$$R_t^k = C_0 t$$

or in logarithmic form

$$\log A = (2/k) \log t + C$$

Here k is known as the kinetic exponent of grain growth, A is the average grain area, and C is a constant. Therefore, the value of the kinetic exponent, k, can be obtained from the slope of the linear regressive line of $\log A$ versus $\log t$.

2.5. Fractal dimension of grain boundary

During the simulation of grain growth, the grain area and grain perimeter in two-dimension or the volume of grain and the surface of grain boundary in three-dimension can also be obtained simultaneously. The fractal dimensions of grains can therefore be acquired by following formula, respectively [19,20].

$$P_G^{1/D} \propto A_G^{1/2}$$

here P_G is the perimeter of grain boundary and A_G is the area of grain in two-dimension;

$$A_G^{1/D} \propto V_G^{1/3}$$

where A_G is the surface area of grain boundary and V_G is the volume of grain in three-dimension. They can be transformed and simplified into logarithmic forms,

$$\log P = D/2 \log A + C_1$$

in two-dimension, and

$$\log A = D/3 \log V + C_2$$

in three-dimension.

3. Results and discussion

3.1. Simulated images of grain growth

Simulated images of grain growth can be easily seen in three-dimension. A grain is showed at different angles and different growth time in Fig. 6. It is obvious that the grain surface is quite rough at early stage of simulation, and that become smooth at later stage of growth.

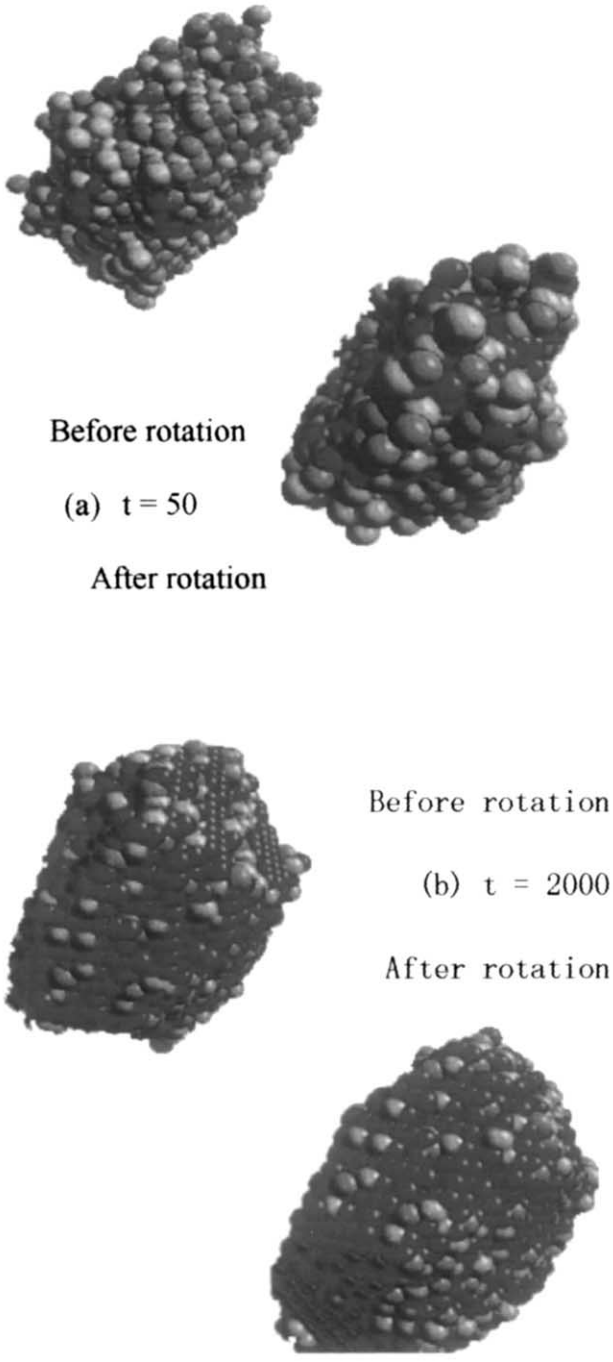

Fig. 6. A grain at different angles and times.

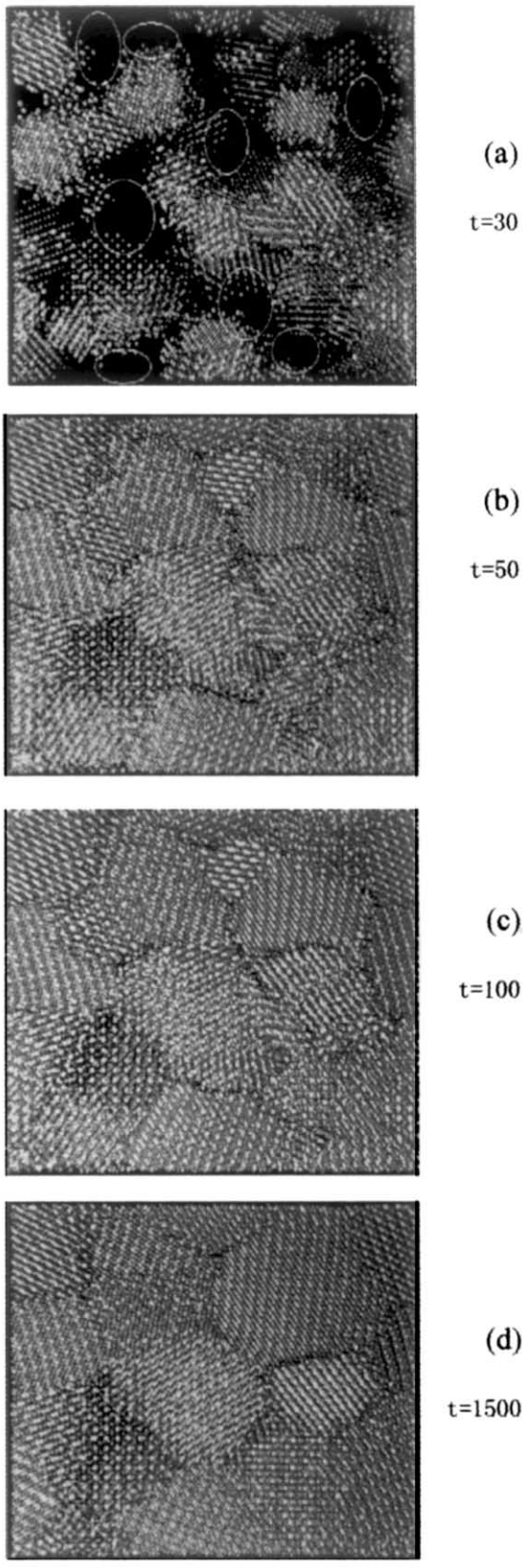

Fig. 7. Sequential images of grain growth in three-dimension.

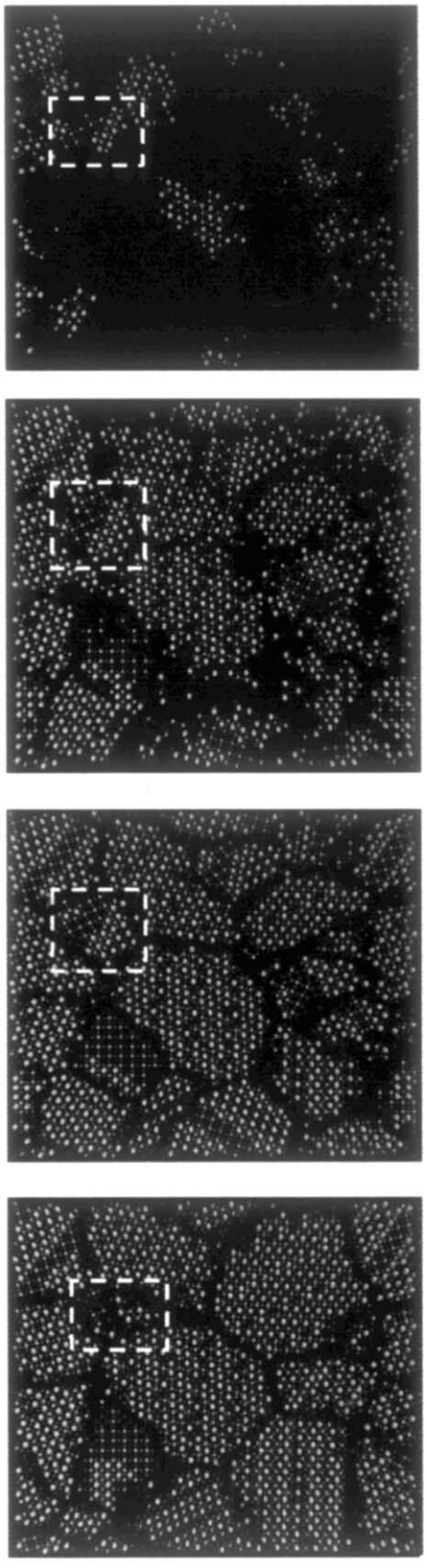

Fig. 8. Sequential images of grain growth in multi-layer.

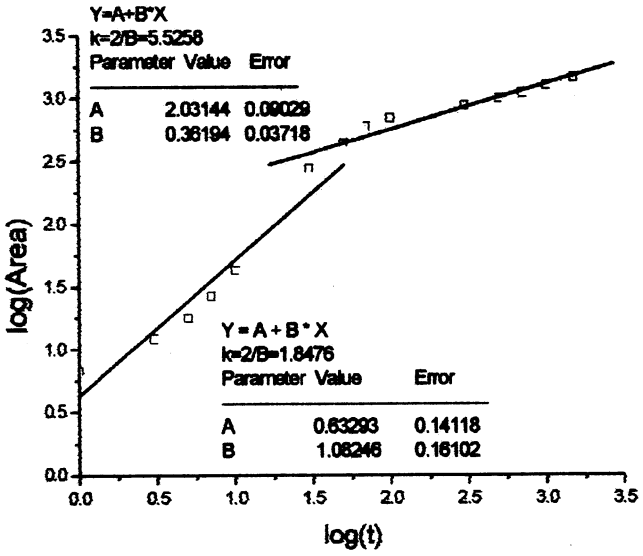

Fig. 9. Average grain area versus time.

Sequential images of grain growth, obtained using the optimized parameters, are shown in Figs. 7(a–d) and 8(a–d). To simulate the images, the values of several parameters are fixed as $N_0 = 10$, $r = 0.10$ nm, $\alpha = 0.25$ and $T = 1300$ °C.

Such realistic images resemble SEM micrograph of $(Ba_{0.9}Sr_{0.1})TiO_3$ ceramics [21]. The evolution of grain microstructure can be seen in the images, which culminates the growth of the seeds eventually adjoining to form grain boundaries.

3.2. Kinetic exponent of grain growth

As all of grain areas can be collected during the simulation, average grain areas in different grains can be calculated. Therefore, the average grain area versus growth time, in logarithm, can be plotted. The kinetic exponents of grain growth correspond inversely to the slope of curve. They are about 1.8 at the early stage of the simulation and then increased towards to 5.5 at the later stage, as shown in Fig. 9. It can be seen that the kinetic exponents of grain growth are actually a function of the time. It is also in good agreement with the experimental results of $(Ba_{0.9}Sr_{0.1})TiO_3$ ceramics [21]. This may be due to that green body, which is to be sintered into ceramic, at the early stage of sintering has higher activation energy than those at the later stage of process.

3.3. Fractal dimensions of grain boundaries

Fig. 10 shows the time dependence of the fractal dimensions of grain boundaries in ceramics simulated. It can be seen that the fractal dimension decrease towards to 2.0, the value for ideal plane, with the time of grain growth. It means that the surfaces of grain boundaries become smoother with growth time, which can be also seen in Fig. 6.

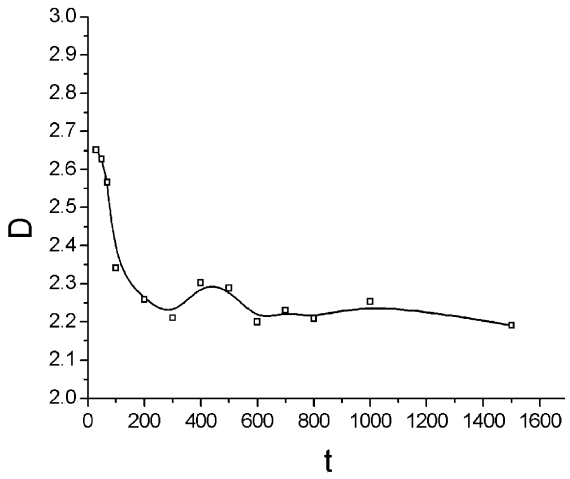

Fig. 10. Time dependence of fractal dimension of grain boundaries.

4. Concluding remarks

The grain growth process of ABO_3 type ceramics was simulated at atomistic level by the Monte Carlo methods with Visual C++ language. Realistic images in series were monitored and quantitative data were obtained during the kinetic evolution of grain growth, including the numbers of ions, lengths and fractal dimensions of grain boundaries in different grains. The resulted kinetic exponents of grain growth were variable, from about 1.8 at the early stage to 5.5 at the later stage of sintering. It was in good agreement with the experimental result of practical $(Ba_{0.9}Sr_{0.1})TiO_3$ ceramics.

References

[1] H.V. Atkinson, Acta Metall 36 (1988) 469.
[2] H.J. Frost, C.V. Thompson, Current Opinion in Solid State and Materials Science, Current Science Ltd., New York, 1996, pp. 361–368.
[3] Y.M. Chiang, D. Birnie, III, W.D. Kingery, Physical Ceramics, Wiley, New York, 1997.
[4] J.E. Burke, D. Turnbull, Prog. Metal Phys. 3 (1952) 220.
[5] R.J. Brook, in: F.F.Y. Wang (Ed.), Ceramic Fabrication Process, Academic Press, New York, 1976, p. 331.
[6] M.P. Anderson, D.J. Srolovitz, G.S. Grest, P.S. Sahni, Acta Metall. 32 (1984) 783.
[7] J.W. Martin, R.D. Doherty, Stability of Microstructure in Metallic Systems, Cambridge University Press, London, 1976.
[8] D.J. Srolovitz, M.P. Anderson, P.S. Sahni, G.S. Grest, Acta Metall. 32 (1984) 793.
[9] M.E. Lines, Principles and Applications of Ferroelectrics and Related Materials, Clarendon Press, Oxford, 1977.
[10] Y.H. Xu, Ferroelectric Materials and Their Applications, Elsevier, Amsterdam, 1991.
[11] R.E. Newnham, Adv. Ceram. Mater. 3 (1988) 12.

[12] S. Nishigaki, T. Nononura, Commun. Am. Ceram. Soc. 71 (1988) C11.
[13] K.Z. Baba-Kishi, D.J. Barber, J. Appl. Cryst. 23 (1990) 43.
[14] M.N. Rahaman, Ceramic Processing and Sintering, Marcel Dekker, New York, 1995.
[15] C.S. Smith, Metal Interfaces, ASM, Cleveland, OH, 1952, p. 65.
[16] W.W. Mullins, J. Appl. Phys. 27 (1956) 900.
[17] P. Feltham, Acta Metall. 5 (1957) 97.
[18] M. Hillert, Acta Metall. 13 (1965) 227.
[19] B.B. Mandelbrot, D.E. Passoja, A.J. Paullay, Nature 308 (1984) 721.
[20] Z.X. Xiong, K.Z. Baba-Kishi, F.G. Shin, in: S.R. Phillpot (Ed.), MRS Proceedings, The Materials Research Society, Boston, 1–4 December, 1997, vol. 492, 1998, pp. 139–144.
[21] Z.X. Xiong, K.Z. Baba-Kishi, F.G. Shin, J. Chin. Ceram. Soc. 29 (2001) 146.